Universal decay rule for reduced widths

D. S. Delion

Horia Hulubei National Institute of Physics and Nuclear Engineering, 407 Atomiştilor, Bucharest-Măgurele 077125, România and Academy of Romanian Scientists, 54 Splaiul Independenţei, Bucharest 050094, România

(Received 8 July 2009; published 20 August 2009)

Emission processes including α decay, heavy cluster decay, and proton and di-proton emission are analyzed in terms of the well-known factorization between the penetrability and the reduced width. By using a shifted harmonic oscillator plus Coulomb cluster-daughter interaction it is possible to derive a linear relation between the logarithm of the reduced width squared and the fragmentation potential, defined as the difference between the Coulomb barrier and the Q value. This relation is fulfilled with a good accuracy for transitions between ground states, as well as for most α decays to low-lying 2^+ excited states. The well-known Viola-Seaborg rule, connecting half-lives with the Coulomb parameter and the product between fragment charge numbers, as well as the Blendowske scaling rule, connecting the spectroscopic factor with the mass number of the emitted cluster, can be easily understood in terms of the fragmentation potential. It is shown that the recently evidenced two regions in the dependence of reduced proton half-lives versus the Coulomb parameter are directly connected with the corresponding regions of the fragmentation potential.

DOI: 10.1103/PhysRevC.80.024310 PACS number(s): 21.10.Tg, 23.50.+z, 23.60.+e, 23.70.+j

I. INTRODUCTION

The family of emission processes triggered by the strong interaction contains various decays, namely particle (proton or neutron) emission, two-proton emission, α-decay, heavy cluster emission, and binary or ternary fission. There are also other nuclear decay processes induced by electromagnetic (γ decay) or weak forces (β decay). The purpose of this work is to investigate only the first type of fragmentation, where the emitted fragments are left in ground or low-lying excited states. They are called cold emission processes and are presently among important tools to study nuclei far from the stability line. Nuclei close to the proton drip line are investigated through proton emission, whereas the neutron drip line region is probed by cold fission processes. On the other hand superheavy nuclei are exclusivelly detected by α-decay chains [1]. Actually the first article in theoretical nuclear physics applying quantum mechanics [2] was devoted to the description of the α decay in terms of the penetration of a preformed particle through the Coulomb barrier.

There are two goals of this article. The first one is to explain the well-known Viola-Seaborg rule [3], valid for all kinds of cold emission processes. It turns out that it is possible to give a simple interpretation of this rule in terms of two physical quantities, namely the Coulomb parameter, connected with the penetrability, and the fragmentation potential, connected with the reduced width. A universal linear dependence between the logarithm of the reduced width and fragmentation potential is derived. It is shown that this interpretation is valid not only for transitions between ground states but also for transitions to excited states. Yet, the scaling dependence of spectroscopic factors in heavy cluster decays versus the mass numbers of the emitted cluster can be also understood in terms of the fragmentation potential.

II. EXPERIMENTAL DECAY RULES

Let us consider a binary emission process $P \to D + C$ from a parent (P) to the daughter nucleus (D) and the lighter cluster (C), which can be in particular an α particle or a proton. The total decay width is the sum of partial decay widths corresponding to different angular momenta, given by [4]

$$\Gamma_l = 2P_l(E_l, r)\gamma_l^2(\beta, r), \tag{2.1}$$

where the standard penetrability and reduced width squared [5] were introduced:

$$\begin{aligned} P_l(E_l, r) &= \frac{\kappa_l r}{\left|H_l^{(+)}(\chi_l, \kappa_l r)\right|^2}, \\ \gamma_l^2(\beta, r) &= \frac{\hbar^2}{2\mu r}\left|s_l^{(\mathrm{int})}(\beta, r)\right|^2. \end{aligned} \tag{2.2}$$

The outgoing spherical Coulomb-Hankel function $H_l^{(+)}(\chi_l, \kappa_l r)$ depends upon two variables, namely the Coulomb (or twice the Sommerfeld) parameter,

$$\chi_l = \frac{Z_D Z_C e^2}{\hbar v_l}, \tag{2.3}$$

and the reduced channel radius, $\rho_l = \kappa_l r$. Here $v_l = \hbar\kappa_l/\mu$ and $\kappa_l = \sqrt{2\mu E_l}/\hbar$ are the asymptotic relative velocity and momentum between the emitted fragments, respectively, in terms of the reduced mass of the daughter-cluster system μ. The center of mass (c.m.) channel energy $E_l = Q - E_l^{(\mathrm{ex})}$ of emitted fragments is also defined, in terms of the difference between the total energy (Q value) and the excitation energy of the daughter nucleus $E_l^{(\mathrm{ex})}$. The internal component $s_l^{(\mathrm{int})}(\beta, r)$ at a certain radius r inside the Coulomb barrier is for deformed emitters a superposition of different Nilsson components multiplied by the propagator matrix [4], depending on deformation parameters β, i.e.,

$$s_l^{(\mathrm{int})}(\beta, r) = \sum_{l'} K_{ll'}(\beta, r) f_{l'}^{(\mathrm{int})}(r). \tag{2.4}$$

For spherical emitters with $K_{ll'} = \delta_{ll'}$ it coincides with the wave function component $f_l^{(\mathrm{int})}(r)$.

The half-life is defined by the inverse of the total decay width, i.e.,

$$T = \frac{\hbar ln2}{\Gamma}. \tag{2.5}$$

Inside the Coulomb barrier the complex Coulomb-Hankel function practically coincides with the real irregular Coulomb function and has a very simple WKB ansatz [4],

$$H_l^{(+)}(\chi,\rho) \approx \frac{\exp[\chi(\arccos\sqrt{x} - \sqrt{x(1-x)})]}{\left(\frac{1}{x}-1\right)^{1/4}} C_l$$
$$\equiv H_0^{(+)}(\chi,\rho) C_l \tag{2.6}$$

where, with the external turning point $r_e = Z_1 Z_2 e^2/E$ and the barrier energy $V_0 = Z_1 Z_2 e^2/r$, the following notations were introduced:

$$x = \frac{\rho}{\chi} = \frac{r}{r_e} = \frac{E}{V_0}$$
$$C_l = \exp\left(\frac{l(l+1)}{\chi}\sqrt{\frac{\chi}{\rho}-1}\right). \tag{2.7}$$

For simplicity, transitions between states with the same angular momentum l were considered here, such as α decays or proton emission processes between ground states. Thus, the logarithm of the so-called reduced half-life, corrected by the exponential centrifugal factor squared C_l^2, defined by the second line of this relation, i.e.,

$$\log_{10} T_{\rm red} = \log_{10} \frac{T}{C_l^2}$$
$$= \log_{10} \frac{\hbar \ln 2}{C_l^2} - \log_{10} 2P_l - \log_{10} \gamma_l^2, \tag{2.8}$$

should be proportional to the Coulomb parameter, i.e.,

$$\log_{10} T_{\rm red} = a_0 \chi + b_0. \tag{2.9}$$

Notice that in most decay processes between ground states one has boson fragments, with zero angular momentum, i.e., $C_l = 1$. The case with $l \neq 0$ is connected with fermions, i.e., proton emission, where $C_l \neq 1$.

The above relation is also called the Geiger-Nuttall law, discovered in 1911 for α decays between ground states (where the angular momentum carried by the α particle is $l = 0$). The explanation of this law was given by Gamow in 1928 [2], in terms of the quantum-mechanical penetration of the Coulomb barrier, i.e., the first line of Eq. (2.2). It is characterized by the Coulomb parameter, which is proportional to the ratio $Z_D/\sqrt{Q_\alpha}$.

The α decays between ground states are characterized by a remarkable regularity, especially for transitions between ground states of even-even nuclei. The fact that α transitions along various isotopic chains lie on separate lines, as stated by the Viola-Seaborg rule [3], i.e.,

$$\log_{10} T = \frac{a_1 Z_D + a_2}{\sqrt{Q_\alpha}} + b_1 Z_D + b_2, \tag{2.10}$$

is connected with different α-particle reduced widths, multiplying the penetrability in Eq. (2.1). From Eq. (2.8) it becomes clear that the reduced width should depend upon the charge

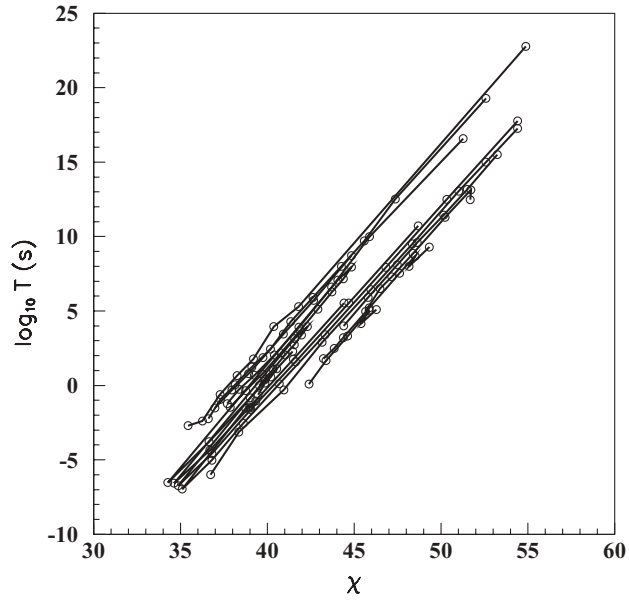

FIG. 1. Logarithm of half lives for α decays from even-even nuclei versus the Coulomb parameter (2.3). Differents lines connect decays from nuclei with the same charge number.

of the daughter nucleus. This feature is shown in Fig. 1. Still in doing systematics along neutron chains there are important deviations with respect to this rule, as for instance in α decay from odd-mass nuclei, and this feature is strongly connected with nuclear structure details. Let us mention that different forms of the Viola-Seaborg relation were used in Refs. [6] and [7].

The Viola-Seaborg rule can be generalized for heavy cluster decays [8], as is shown in Fig. 2. Here the angular momenta carried by emitted fragments are zero. In Ref. [9] the following generalized Viola-Seaborg rule for the heavy cluster emission was proposed,

$$\log_{10} T = a_1 \frac{Z_D Z_C}{\sqrt{Q}} + a_2 Z_D Z_C + b_2 + c_2, \tag{2.11}$$

with the following set of parameters,

$$a_1 = 1.517, \quad a_2 = 0.053, \quad b_2 = -92.911,$$
$$c_2 = 0\,(\text{even}), \; = 1.402\,(\text{odd}),$$

where c_2 is the blocking parameter for odd-mass nuclei. Thus, from Eq. (2.8) the reduced width in this case should depend upon the product between daughter and cluster charges.

An interesting feature can be seen in Fig. 3 where the logarithm of the reduced half-life (2.8) versus the Coulomb parameter for various proton emitters is plotted [10,11]. In this case most of emitters have nonvanishing angular momentum. The data are roughly divided into two regions, corresponding to $Z < 68$ (open circles) and $Z > 68$ (solid circles). This pattern can be assimilated with a generalized Viola-Seaborg rule for the two groups of charge numbers.

The situation with binary cold fission is quite different. Here there is not a simple linear dependence between the half-life for a given isotopic partition and the Coulomb parameter, because mass asymmetry changes during the scission process.

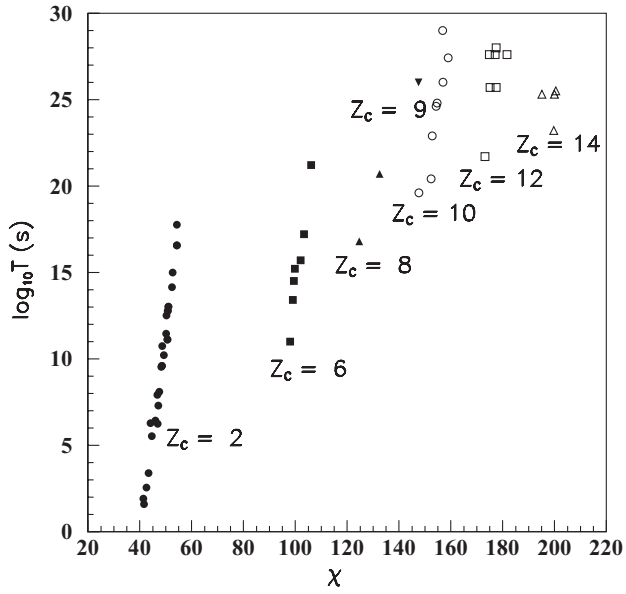

FIG. 2. Logarithm of half-lives for heavy cluster decays and the corresponding α decays from the same mother nuclei versus the Coulomb parameter (2.3). Differents symbols denote the charge number of the emitted cluster.

III. A SIMPLE MODEL FOR THE REDUCED WIDTH

The decay processes can be schematically described by the following cluster-daugher spherical potential:

$$V(r) = \hbar\omega\frac{\beta(r-r_0)^2}{2} + v_0, \quad r \leqslant r_B$$
$$= \frac{Z_D Z_C e^2}{r} \equiv V_C(r), \quad r > r_B, \tag{3.1}$$

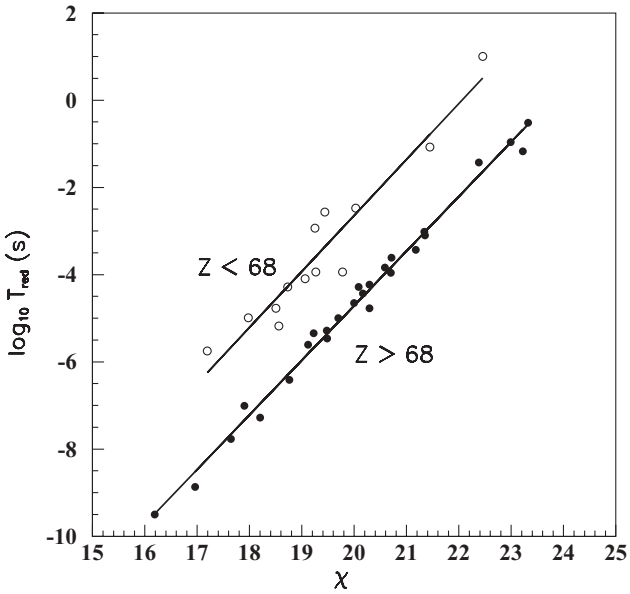

FIG. 3. Logarithm of reduced half-lives (2.8) for proton emitters versus the Coulomb parameter (2.3). Open circles denote emitters with $Z < 68$, while solid circles denote emitters with $Z > 68$.

where $r_0 = 1.2A_D^{1/3}$ is the surface radius of the daughter nucleus. Indeed, microscopic calculations have shown that the preformation factor of the α particle has a Gaussian shape, centered on the nuclear surface [12]. Moreover, the spherical component of the preformation amplitude gives more than 90% contribution in the α-decay width of deformed nuclei. Notice that the radial equation of the shifted harmonic oscillator (ho) potential is similar to the equation of the one-dimensional oscillator, but has approximate eigenvalues given by

$$E_{nl} = \hbar\omega\left(n + \frac{1}{2}\right) + \frac{\hbar^2 l(l+1)}{2\mu r_0^2}. \tag{3.2}$$

By considering the Q value as the first eigenstate in the shifted ho well $Q - v_0 = \frac{1}{2}\hbar\omega$, together with the continuity condition at the top of the barrier r_B, one obtains the following relation:

$$\hbar\omega\frac{\beta(r_B - r_0)^2}{2} = V_{\rm frag}(r_B) + \frac{1}{2}\hbar\omega, \tag{3.3}$$

where the so-called fragmentation (or driving) potential was introduced as the difference between the top of the Coulomb barrier and the Q value,

$$V_{\rm frag}(r_B) = V_C(r_B) - Q. \tag{3.4}$$

The second component in Eq. (2.8) contains the logarithm of the Coulomb-Hankel function inside the Coulomb barrier which, according to Eq. (2.6), is proportional to the Colomb parameter χ. The third part contains the reduced width squared which, according to Eq. (2.2), is proportional to the modulus of the internal wave function squared. For a shifted ho well one has for the ground state

$$\left|f_0^{(\rm int)}(r)\right|^2 = A_0^2 e^{-\beta(r-r_0)^2}. \tag{3.5}$$

By using the notation $\gamma \equiv \gamma_0$ and Eq. (3.3) one obtains the following relation,

$$\log_{10}\gamma^2(r_B) = -\frac{\log_{10} e^2}{\hbar\omega}V_{\rm frag}(r_B) + \log_{10}\frac{\hbar^2 A_0^2}{2e\mu r_B}. \tag{3.6}$$

In this way one determines that indeed the logarithm of the half-life is of the Viola-Seaborg type,

$$\log_{10} T = c_1(r_B)\chi + c_2 V_{\rm frag}(r_B) + c_3\left(r_B, A_0^2\right), \tag{3.7}$$

because the fragmentation potential contains the product $Z_D Z_C$. Its coefficient depends upon the touching radius, but this radius has a very small variation along various isotopic chains. Notice that the slope in Eq. (3.6) has a negative value and it is connected with the shape of the interaction potential (ho energy $\hbar\omega$), whereas the free term gives information about the amplitude of the cluster wave function.

Our calculation has shown that the linear relation, Eq. (3.6), but with different coefficients, remains valid in the most general case of the double folding plus repulsive interaction between fragments, used in Refs. [13] and [14].

IV. DECAY RULE FOR REDUCED WIDTHS

Most of the experimental data refer to the α decay. Therefore, there were analyzed reduced widths in α decays

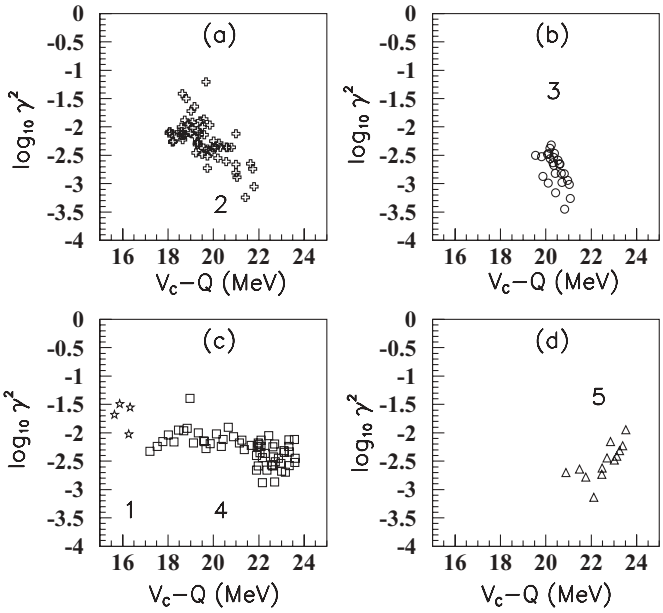

FIG. 4. The logarithm of the α-decay reduced width squared versus the fragmentation potential (3.4) for regions of the nuclear chart described by Eq. (4.1).

connecting ground states of even-even nuclei. In Fig. 4 the logarithm of the experimental reduced width squared is plotted by using the above relation versus the fragmentation potential. The data are divided into five regions of even-even α emitters as follows:

(1) $Z < 82$, $50 < N < 82$, Fig. 4(c), stars;
(2) $Z < 82$, $82 < N < 126$, Fig. 4(a), crosses;
(3) $Z > 82$, $82 < N < 126$, Fig. 4(b), circles; (4.1)
(4) $Z > 82$, $126 < N < 152$, Fig. 4(c), squares;
(5) $Z > 82$, $N > 152$, Fig. 4(d), triangles.

In calculations the value of the touching radius was used, i.e.,

$$r_B = 1.2\left(A_D^{1/3} + A_C^{1/3}\right), \tag{4.2}$$

where the approximation $K_{ll'} \approx \delta_{ll'}$ in Eq. (2.4) is fulfilled with 90% accuracy for the most deformed nuclei [4]. Notice that regions 1–4 contain rather long isotopic chains, whereas region 5 contains not more than two isotopes/chain. This is the reason why, except for region 5, the reduced width decreases with respect to the fragmentation potential, according to the theoretical prediction given by Eq. (3.6). Notice that in regions 1 and 4, above ^{100}Sn and ^{208}Pb double-magic emitters, respectively, the ho parameter of the α-daughter potential is larger than that for regions 2 and 3, corresponding to charge numbers around the double-magic nucleus ^{208}Pb. However, one obtains the largest amplitudes of the cluster wave function in regions 2 and 3.

An interesting observation can be made from Fig. 5, where the difference $T_{\rm cor} = \log_{10} T - c_2 V_{\rm frag}(r_B) - c_3(r_B, A_0^2)$ versus the Coulomb parameter χ is plotted; the same five symbols for the above-described regions are used. Amazingly enough three lines corresponding to different amplitudes of

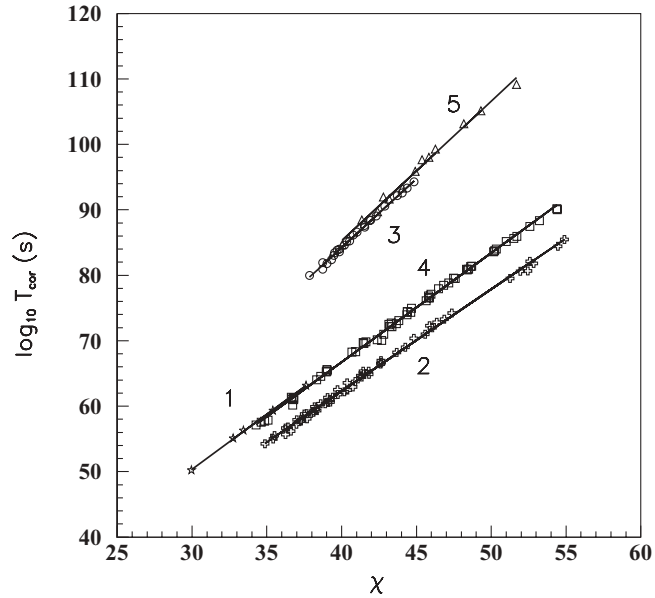

FIG. 5. The difference $\log_{10} T - c_2 V_{\rm frag}(r_B) - c_3$ versus the Coulomb parameter χ for five different regions described by Eq. (4.1). The straight lines are the corresponding linear fits.

the cluster wave function were obtained. Regions 1 and 4, corresponding to emitters above double-magic nuclei ^{50}Sn and ^{208}Pb, respectively, have practically the same internal amplitudes, A_0. The same is true for regions 3 and 5.

The linear dependence of $\log_{10} \gamma^2$ versus the fragmentation potential (3.6) remains valid for any kind of cluster emission. This fact is nicely confirmed by heavy cluster emission processes in Fig. 6(a), which shows the dependence between

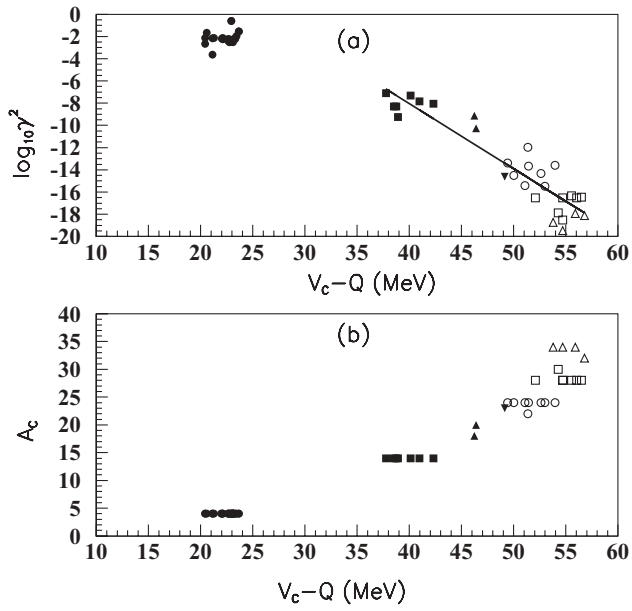

FIG. 6. (a) The logarithm of the reduced width squared versus the fragmentation potential (3.4). Different symbols correspond to cluster decays in Fig. 2. The straight line is the linear fit (4.3) for cluster emission processes, except α decay. (b) Cluster mass number versus the fragmentation potential.

the corresponding experimental values for the same decays in Fig. 2. Here a similar dependence for α decays corresponding to the same heavy cluster emitters is plotted. The straight line is the linear fit for cluster emission processes, except α decays

$$\log_{10}\gamma^2 = -0.586(V_C - Q) + 15.399. \tag{4.3}$$

The above value of the slope $-\log_{10} e^2/\hbar\omega$ in Eq. (3.6) leads to $\hbar\omega \approx 1.5$ MeV, with the same order of magnitude as in the α-decay case. The relative large scattering of experimental data around the straight line in Fig. 6 can be explained by the simplicity of the used cluster-core potential (3.1).

Let us mention that a relation expressing the spectroscopic factor (proportional to the reduced width) for cluster emission processes was derived in Ref. [15],

$$S = S_\alpha^{(A_C-1)/3}, \tag{4.4}$$

where A_C is the mass of the emitted light cluster and $S_\alpha \sim 10^{-2}$. As can be seen from Fig. 6(b) between A_C and $V_{\rm frag}$ there exists a rather good linear dependence and therefore the above scaling law can be easily understood in terms of the fragmentation potential.

Concerning the reduced widths of proton emitters in Refs. [11] and [16], note the correlation between the reduced width and the quadrupole deformation. This fact can be seen in Fig. 7(a), where the region with $Z < 68$ corresponds to $\beta > 0.1$ (open circles), whereas the other one with $Z > 68$ corresponds to $\beta < 0.1$ (solid circles). The two linear fits have obviously different slopes. This dependence is induced by the propagator matrix $K_{ll'}(\beta, r)$ in Eq. (2.4). Notice that the two solid circles with the smallest reduced widths correspond to the heaviest emitters with $Z > 80$.

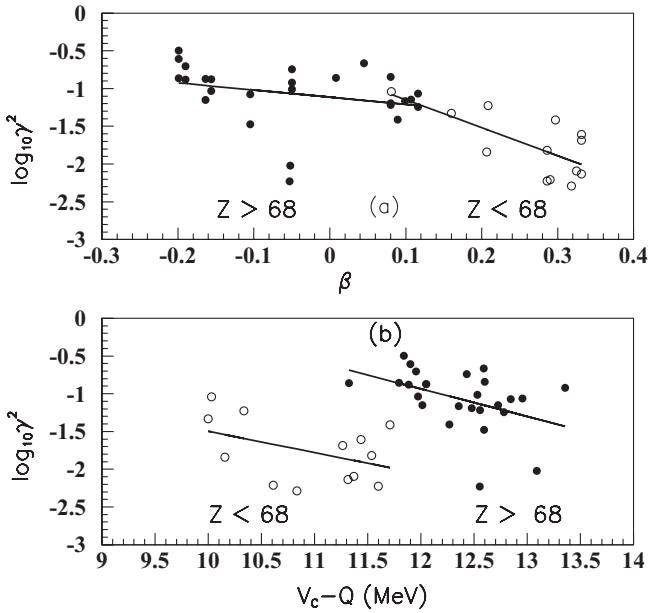

FIG. 7. (a) The logarithm of the reduced width squared versus the quadrupole deformation. Open circles denote emitters with $Z < 68$, whereas dark circles denote emitters with $Z > 68$ for proton emission. The two regression lines fit the corresponding data. (b) The logarithm of the reduced width squared versus the fragmentation potential (3.4). The symbols are the same as those in panel (a).

At the same time one can see from Fig. 7(b) that the same data are clustered into two regions, which can be directly related with the fragmentation potential (3.4). Here the two linear fits in terms of the fragmentation potential, corresponding to the two regions of charge numbers, have roughly the same slopes, but different values in origin. Thus, the two different lines in Fig. 3 can be directly connected with similar lines in Fig. 7(b). They correspond to different orders of magnitude of the fragmentation potential, giving different orders to wave functions and therefore to reduced widths.

A special case is given by the two-proton emission. This process was predicted a long time ago [17], but only a few such emitters have been recently detected until now. Let us mention that the most recent general treatment of the two-proton emission process, assuming a three-body dynamics, is given in Ref. [18] (and the references therein).

The experimental half-lives versus the Coulomb parameter are denoted in Fig. 8(a) by triangles. The emitter charges are also pointed out. Here a simplified version is assumed, where the light emitted cluster is supposed to be a di-proton with the charge $Z_C = 2$. In this case one can use the factorization of the decay width (2.1). One sees that half-lives (triangles) follow the general trend (dashed line) of the usual proton emitters, denoted in the same figure by the same symbols used in Fig. 3. Figure 8(b) plots the logarithm of the reduced width squared versus the fragmentation potential by triangles. One indeed observes that the slope of the fitting dashed line has a negative value $-\log_{10} e^2/\hbar\omega$, but with a much larger value in comparison with proton emitters, given by the same symbols as those used in Fig. 7(b). The three lines in this

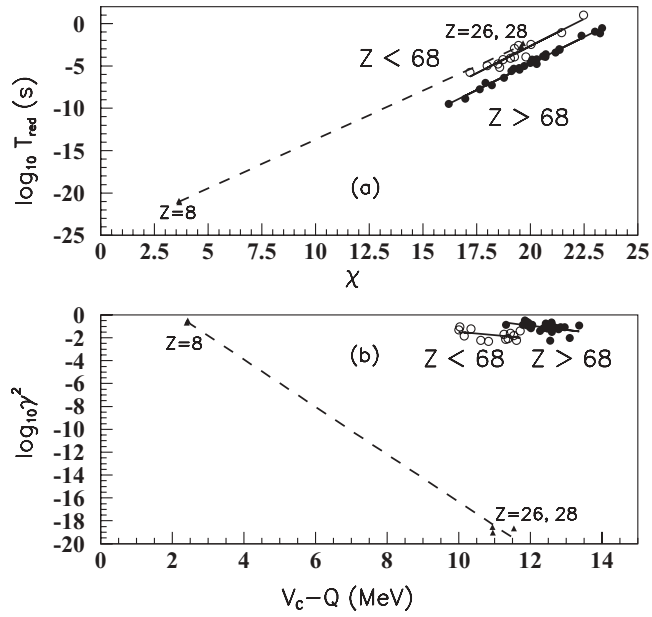

FIG. 8. (a) The logarithm of the half-life versus the Coulomb parameter for two-proton emitters (triangles). Circles denote data for proton emitters in Fig. 3. (b) The logarithm of the reduced width squared versus the fragmentation potential (3.4) for two-proton emitters (triangles). The same quantity denoted by circles for proton emitters in Fig. 7(b). The solid lines fit proton data, while the dashed lines fit two-proton data.

figure, corresponding to proton and two-proton radioactivity, respectively, are given by

$$\begin{aligned} \log_{10}\gamma^2 &= -0.283(V_C - Q) + 1.329, \quad Z < 68 \\ \log_{10}\gamma^2 &= -0.365(V_C - Q) + 3.440, \quad Z > 68 \\ \log_{10}\gamma^2 &= -2.075(V_C - Q) + 4.403. \end{aligned} \tag{4.5}$$

The ho energy is $\hbar\omega \approx 1.5$ MeV for proton emission (i.e., the same order as for heavy cluster radioactivity and α decay) and $\hbar\omega \approx 0.2$ MeV for two-proton emission, by considering the di-proton approximation. This small ho energy is connected with the use of Eq. (4.2) in estimating the spatial extension of the di-proton system R_C and therefore the fragmentation potential. In reality the di-proton is not a bound system and it changes its size during the barrier penetration. Our microscopic estimate, by using a pairing residual interaction between emitted protons from ^{45}Fe, evidenced that the size of the wave packet increases in the relative coordinate by 1 fm over a distance of 1 fm in the region of the nuclear surface. Actually the reduced width defined by Eq. (2.1) can be generalized by using the other extreme scenario, given by a sequential emission, where this relation is integrated over all possible energies of emitted particles [19].

An interesting observation concerns the amplitude A_0 in Eq. (3.6), given by the value of fitting lines in origin. It has similar values for both two-proton and proton emitters with $Z > 68$.

Now let us analyze α-decay processes to excited low-lying 2^+ states. More than 70 decays of even-even rotational, vibrational, and transitional nuclei were considered [13,14]. The hindrance factor (HF) is defined as the ratio of reduced widths squared connecting the ground states and ground to excited states with the angular momentum $l = 2$, i.e.,

$$\mathrm{HF} = \frac{\gamma_0^2}{\gamma_2^2}. \tag{4.6}$$

Thus, by using Eq. (3.6), the logarithm of the HF becomes proportional to the excitation energy of the daughter nucleus,

$$\log_{10}\mathrm{HF} = \frac{\log_{10} e^2}{\hbar\omega} E_2^{(\mathrm{ex})} + \log_{10}\frac{A_0^2}{A_2^2}. \tag{4.7}$$

It is worth mentioning that this relation is equivalent to the Boltzman distribution for the reduced width to the excited state γ_2. In Refs. [20] and [21] such a dependence was postulated to describe HF's.

In Fig. 9 the logarithm of the HF versus the excitation energy for rotational nuclei with $E_2^{(\mathrm{ex})} < 0.1$ MeV is plotted, by using the same notations given by Eq. (4.1). As a rule the HF's have small values and therefore the wave functions have similar amplitudes, $A_0 \approx A_2$. Notice that region 4 in Fig. 9(a), with $Z > 82$ and $126 < N < 126$, contains most of the rotational emitters (33 out of 41). Moreover, our analysis has shown that here the HF has an almost constant value along various isotopic chains, because the energy range is very short (about 100 keV).

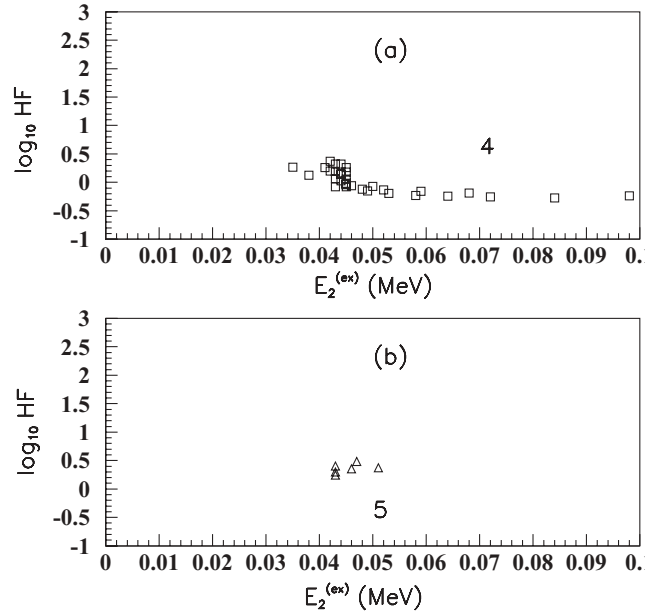

FIG. 9. The logarithm of the hindrance factor versus the excitation energy of the daughter nucleus for rotational nuclei. The symbols and numbers correspond to the regions given in Eq. (4.1).

In Fig. 10 the same quantity as in Fig. 9 is given, but for transitional and vibrational nuclei, with $E_2^{(\mathrm{ex})} > 0.1$ MeV. The situation looks here to be different and more complex, with respect to rotational nuclei. The best example is given by the same region 4 in Fig. 10(c), where the slope has a positive value, as predicted by Eq. (4.7). Notice that this region contains almost half of the analyzed vibrational emitters (14 out of 31).

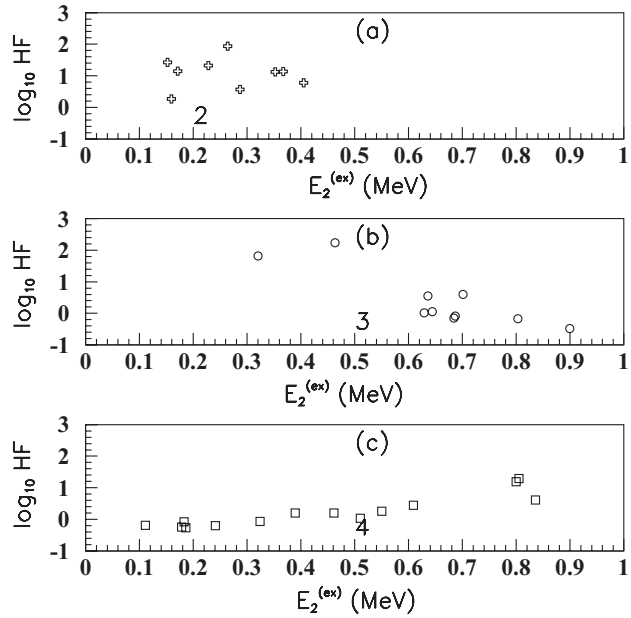

FIG. 10. The same as in Fig. 9, but for transitional and vibrational nuclei.

V. CONCLUSIONS

Cold emission processes, in terms of the well-known factorization of the decay width between the penetrability and reduced width squared, were analyzed. Based on a simple model of the two-body dynamics, namely a shifted harmonic oscillator potential surounded by the Coulomb interaction, a universal analytical relation expressing the logarithm of the reduced width squared as a linear function in terms of the fragmentation potential (defined as the difference between the Coulomb barrier and the Q value) was derived. Notice that the slope has the same order of magnitude, corresponding to a ho energy $\hbar\omega \approx 1.5$ MeV, for all decay processes, except the di-proton emission, where the factorization (2.1) is not anymore valid. This rule is a consequence of the fact that the logarithm of the wave function squared is proportional to the difference between the height of the Coulomb potential at a given radius and the energy of the system. It is fulfilled with a reasonable accuracy by experimental data, describing transitions between ground states as well as for α transitions to excited states in the most relevant region with $Z > 82$ and $126 < N < 152$. As a particular case, the two regions in the dependence of proton emitter half-lives, corrected by the centrifugal barrier, versus the Coulomb parameter are directly related with the corresponding regions of the fragmentation potential. Thus, the clustering character of the wave function inside the Coulomb barrier (i.e., the fragments are already preformed here) is evidenced by this linear rule in terms of the fragmentation potential. Yet the well-known scaling relation, connecting the spectroscopic factor with the mass of the emitted cluster, can be nicely explained in terms of the fragmentation potential.

ACKNOWLEDGMENTS

This work was supported by Contract IDEI-119 of the Romanian Ministry of Education and Research.

[1] Y. K. Gambhir, A. Bhagwat, and M. Gupta, Ann. Phys. (NY) **320**, 429 (2005).
[2] G. Gamow, Z. Phys. **51**, 204 (1928).
[3] V. E. Viola and G. T. Seaborg, J. Inorg. Nucl. Chem. **28**, 741 (1966).
[4] D. S. Delion, R. J. Liotta, and R. Wyss, Phys. Rep. **424**, 113 (2006).
[5] A. M. Lane and R. G. Thomas, Rev. Mod. Phys. **30**, 257 (1958).
[6] Y. Hatsukawa, H. Nakahara, and D. C. Hoffman, Phys. Rev. C **42**, 674 (1990).
[7] B. A. Brown, Phys. Rev. C **46**, 811 (1992).
[8] D. N. Poenaru, Y. Nagame, R. A. Gherghescu, and W. Greiner, Phys. Rev. C **65**, 054308 (2002).
[9] Z. Ren, C. Xu, and Z. Wang, Phys. Rev. C **70**, 034304 (2004).
[10] A. A. Sonzogni, Nucl. Data Sheets **95**, 1 (2002).
[11] D. S. Delion, R. J. Liotta, and R. Wyss, Phys. Rev. Lett. **96**, 072501 (2006).
[12] D. S. Delion, A. Insolia, and R. J. Liotta, Phys. Rev. C **46**, 1346 (1992).
[13] S. Peltonen, D. S. Delion, and J. Suhonen, Phys. Rev. C **75**, 054301 (2007).
[14] S. Peltonen, D. S. Delion, and J. Suhonen, Phys. Rev. C **78**, 034608 (2008).
[15] R. Blendowske, T. Fliessbach, and H. Walliser, Z. Phys. A **339**, 121 (1991).
[16] E. L. Medeiros, M. M. N. Rodrigues, S. B. Duarte, and O. A. P. Tavares, Eur. Phys. J. A **34**, 417 (2007).
[17] V. I. Goldansky, Nucl. Phys. **19**, 482 (1960).
[18] L. V. Grigorenko and M. V. Zhukov, Phys. Rev. C **76**, 014008 (2007); **76**, 014009 (2007).
[19] R. A. Kryger *et al.*, Phys. Rev. Lett. **74**, 860 (1995).
[20] C. Xu and Z. Ren, Phys. Rev. C **75**, 044301 (2007).
[21] Y. Z. Wang, H. F. Zhang, J. M. Dong, and G. Royer, Phys. Rev. C **79**, 014316 (2009).